Inorg. Chem. **2008**, *47*, 6633−6644

Electron Paramagnetic Resonance and Density-Functional Theory Studies of Cu(II)-*bis*(oxamato) Complexes

Björn Bräuer,*,† Florian Weigend,‡ Maria Fittipaldi,§,⊥ Dante Gatteschi,§,⊥ Edward J. Reijerse,|| Annalisa Guerri,⊥ Samuele Ciattini,⊥ Georgeta Salvan,† and Tobias Rüffer†

Department of Chemistry, Chemnitz University of Technology, 09107 Chemnitz, Germany, Forschungszentrum Karlsruhe, Institute for Nanotechnology, 76021 Karlsruhe, Germany, Department of Chemistry and INSTM, University of Florence, 50019 Sesto Fiorentino, Florence, Italy, and Max-Planck Institut für Bioanorganische Chemie, 45470 Mülheim an der Ruhr, Germany

Received December 20, 2007

In this work we present the investigation of the influence of electronic and structural variations induced by varying the *N,N′*-bridge on the magnetic properties of Cu(II)-*bis*(oxamato) complexes. For this study the complexes $[Cu(opba)]^{2-}$ (**1**, opba = *o*-phenylene-*bis*(oxamato)), $[Cu(nabo)]^{2-}$ (**2**, nabo = 2,3-naphthalene-*bis*(oxamato)), $[Cu(acbo)]^{2-}$ (**3**, acbo = 2,3-anthrachinone-*bis*(oxamato)), $[Cu(pba)]^{2-}$ (**4**, pba = propylene-*bis*(oxamato)), $[Cu(obbo)]^{2-}$ (**5**, obbo = o-benzyl-*bis*(oxamato)), and $[Cu(npbo)]^{2-}$ (**6**, npbo = 1,8-naphthalene-*bis*(oxamato)), and the respective structurally isomorphic Ni(II) complexes (**8**−**13**) have been prepared as $(^{n}Bu_4N)^{+}$ salts. The new complex $(^{n}Bu_4N)_2[Cu(R\text{-}bnbo)]\cdot 2H_2O$ (**7**, R-bnbo = (R)-1,1′-binaphthalene-2,2′-*bis*(oxamato)) was synthesized and is the first chiral complex in the series of Cu(II)-bis(oxamato) complexes. The molecular structure of **7** has been determined by single crystal X-ray analysis. The Cu(II) ions of the complexes **1**−**7** are $\eta^4(\kappa^2N, \kappa^2O)$ coordinated with a more or less distorted square planar geometry for **1**−**6** and a distorted tetrahedral geometry for **7**. Using pulsed Electron Nuclear Double Resonance on complex **6**, detailed information about the relative orientation of the hyperfine (**A**) and nuclear quadrupole tensors (**Q**) of the coordinating nitrogens with respect to the *g* tensor were obtained. Electron Paramagnetic Resonance studies in the X, Q, and W-band at variable temperatures were carried out to extract *g* and *A* values of N ligands and Cu ion for **1**−**7**. The hyperfine values were interpreted in terms of spin population on the corresponding atoms. The obtained trends of the spin population for the monomeric building blocks were shown to correlate to the trends obtained in the dependence of the exchange interaction of the corresponding trinuclear complexes on their geometry.

1. Introduction

Because of their large structural variability, Cu(II)-*bis*(oxamato) complexes have been used as precursors for the synthesis of multimetallic complexes (see, e.g., refs 1, 2) or as building blocks for two and three-dimensional magnetic networks[3] and for single molecule magnets.[4,5] Their structural variability makes them also excellently suited for basic research studies of magnetic superexchange phenomena (see, e.g., refs 2, 6).

One example is the synthesis of trinuclear Cu(II)-*bis*(oxamato) complexes possessing 5-fold coordinated Cu(II) ions in their terminal position.[2] The magnetic superexchange interaction, described by the J ($H = -J\mathbf{S}_A\cdot\mathbf{S}_B$) parameter,

* To whom correspondence should be addressed. E-mail: bbj@hrz.tu-chemnitz.de.
† Chemnitz University of Technology.
‡ Forschungszentrum Karlsruhe, Institute for Nanotechnology.
§ INSTM
|| Max-Planck Institut für Bioanorganische Chemie.
⊥ Department of Chemistry, University of Florence.

(1) Kahn, O. *Molecular Magnetism*; VCH: Weinheim, 1993.
(2) Costa, R.; Garcia, A.; Ribas, J.; Mallah, T.; Journaux, Y. *Inorg. Chem.* **1993**, *32*, 3733.
(3) Stumpf, H. O.; Ouahab, L.; Pei, Y.; Grandjean, D.; Kahn, O. *Science* **1993**, *261*, 447.
(4) Dias, A. C.; Knobel, M.; Stumpf, H. O. *J. Magn. Magn. Mater.* **2001**, *226*, 1961.
(5) Pereira, C. L. M.; Pedroso, E. F.; Novak, M. A.; Brandl, A. L.; Knobel, M.; Stumpf, H. O. *Polyhedron* **2003**, *22*, 2387.
(6) Costa, R.; Garcia, A.; Sanchez, R.; Ribas, J.; Solans, X.; Rodriguez, V. *Polyhedron* **1993**, *12*, 2697.

10.1021/ic702460t CCC: $40.75
Published on Web 07/02/2008

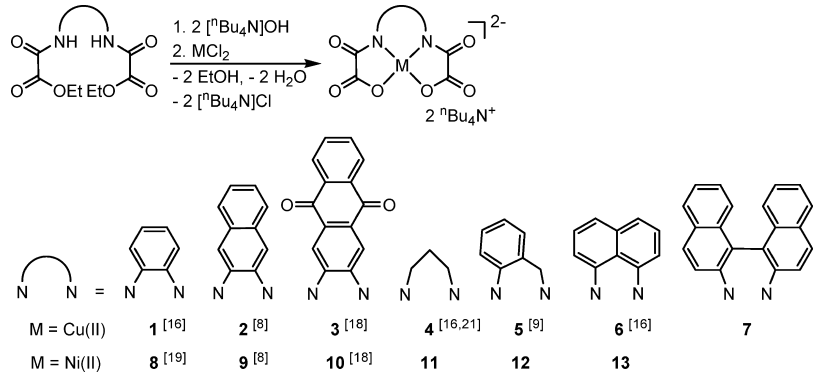

Figure 1. Synthesis strategy of metal-*bis*(oxamato) complexes.

depends strongly on the coordination geometry around the terminal Cu(II) ions. To quantify the correlation between the structural and magnetic properties, the geometrical parameter τ was introduced, which is 0 in the case of an ideal square pyramidal and 1 for an ideal trigonal bipyramidal coordination geometry.[7] It was shown that there is a linear dependence of J on τ.[2,6]

Recently, the magnetic superexchange coupling parameters J of $[Cu_3(opba)(pmdta)_2](NO_3)_2$ (**15**), $[Cu_3(nabo)(pmdta)_2](BF_4)_2$ (**16**), and $[Cu_3(obbo)(pmdta)_2](NO_3)_2$ (**17**) with pmdta = *N,N,N′,N″,N″*-pentamethyldiethylenetriamine were studied.[8–10] The complexes **15**, **16**, and **17** correspond to **1**, **2**, and **5**, see Figure 1, as starting material, respectively. Because structural aspects strongly influence the spin distribution in the mononuclear precursor molecules, it is reasonable to assume that they also affect the magnitude of the magnetic super exchange interactions between neighboring transition metals of the corresponding trinuclear complexes. Therefore, these complexes can be used as model systems to find a relation between the spin population distribution of the mononuclear precursors and the J of the corresponding trinuclear complexes.

To study the influence of the deviation from the square planar coordination geometry and the N−Cu−N bond angle on the spin population distribution, we have synthesized the Cu(II)-(R)-1,1′-binaphthalene-2,2′-*bis*(oxamato) complex (**7**) with a N_2O_2 donor set that imposes a strong tetrahedral distortion due to steric reasons. This kind of complexes is highly interesting because distorted square planar coordination geometry is known to be present also in some metalloenzymes and metalloproteins.[11–13] Furthermore, the J parameter of the corresponding trinuclear complex of **7** was evaluated by density-functional theory (DFT) calculations to investigate the influence of the spin population distribution on the J parameter.

The spin population is commonly determined by means of high resolution X-ray and polarized neutron diffraction measurements, respectively. In the case of *bis*(oxamato) class of transition metal complexes, the combination of these two methods has been successfully applied for studying the ferrimagnetic chain compound MnCu(pba)-$(H_2O)_3 \cdot 2H_2O$ (pba = 1,3-propylene-*bis*(oxamato).[14,15] Complementary information can be obtained through magnetic resonance techniques.

In this work we show that continuous wave Electron Paramagnetic Resonance (EPR) in the X, Q, and W-band and pulsed Electron Nuclear Double Resonance (ENDOR) techniques at variable temperatures can be applied to extract detailed information about the spin population distribution of the mononuclear building blocks.

2. Experimental Section

2.1. Synthesis of the Complexes. All the starting chemicals and solvents were purchased from commercial sources. For crystallization, the powdered substances were dissolved in acetonitrile and then crystallized under aerobic conditions in closed systems by slow condensation of Et_2O. The compounds **1**−**13** shown in Figure 1 were synthesized according to or in analogy to literature procedures.[8,16–20] The structural properties of compounds **1**−**7** are reported in Table 1.

Preparation of 7. $[^nBu_4N]_2[Cu(R\text{-}bnbo)] \cdot 2H_2O$ (**7**) was obtained from (R)-diethyl-*N,N′*-1,1′-binaphthalene-2,2′-*bis*(oxamate) (**14**) which was prepared from ethyloxalylchloride and (R)-2,2′-diamino-1,1′-binaphthalene by literature methods.[22]

Complex **7** was prepared as follows. To a solution of **14** (241 mg, 0.5 mmol) in MeOH (60 mL) was added $^nBu_4NOH$ (1.31 g of

(7) Mutterkies, E. L.; Guggenberger, L. J. *J. Am. Chem. Soc.* **1974**, *96*, 6–1748.
(8) Rüffer, T.; Bräuer, B.; Powell, A.; Hewitt, I.; Salvan, G. *Inorg. Chim. Acta* **2007**, *360*, 11–3475.
(9) Rüffer, T.; Bräuer, B.; Meva, F. E.; Walfort, B.; Salvan, G.; Powell, A. K.; Hewitt, I. J.; Sorace, L.; Caneschi, A. *Inorg. Chim. Acta* **2007**, *360, 12*, 3777.
(10) Bräuer, B.; Weigend, F.; Totti, F.; Zahn, D. R. T., Rüffer, T., Salvan, G., *J. Phys. Chem. B.* **2008**, *112*, 5585.
(11) Bencini, A.; Gatteschi, D.; Zanchini, C. *J. Am. Chem. Soc.* **1980**, *102*, 5234.
(12) Colman, P. M.; Freeman, H. C.; Guss, J. M.; Murata, M.; Norris, V. A.; Ramshan, J. A. M.; Venkatappa, M. P. *Nature (London)* **1978**, *272*, 319.
(13) Solomon, E. I. *Inorg. Chem.* **2006**, *45*, 8012.
(14) Pillet, S.; Souhassou, M.; Mathonière, C.; Lecomte, C. *J. Am. Chem. Soc.* **2004**, *126*, 1219.
(15) Baron, V.; Gillon, B.; Cousson, A.; Mathoniere, C.; Kahn, O.; Grand, A.; Ohrstrom, L.; Delley, B.; Bonnet, M.; Boucherle, J. X. *J. Am. Chem. Soc.* **1997**, *119*, 3500.
(16) Cervera, B.; Sanz, J. L.; Ibanez, M. J.; Vila, G.; Lloret, F.; Julve, M.; Ruiz, R.; Ottenwaelder, X.; Aukauloo, A.; Poussereau, S.; Journaux, Y.; Munoz, M. C. *J. Chem. Soc., Dalton Trans.* **1998**, 781.
(17) Bräuer, B.; Rüffer, T.; Kirmse, R.; Griebel, J.; Weigend, F.; Salvan, G. *Polyhedron* **2007**, *26*, 1773.
(18) Rüffer, T.; Bräuer, B.; Meva, F., Walfort, B., submitted for publication.
(19) Gao, E.-Q.; Liao, D.-Z.; Jiang, Z.-H.; Yan, S.-P. *Acta Crystallogr., Sect. C: Cryst. Struct. Commun.* **2001**, *57*, 807.
(20) Fettouhi, M.; Ouahab, L.; Boukhari, A.; Cador, O.; Mathoniere, C.; Kahn, O. *Inorg. Chem.* **1996**, *4932*, 35.

Table 1. Structural Properties of Different Cu(II)-*bis*(oxamato) Complexes

complex	**1**	**2**	**3**	**4**	**5**	**6**	**7**
d(Cu−N)/Å[a]	1.886(2)	1.887(2)	1.902(2)	1.904(3)	1.889(2)[a] 1.921(2)[b]	1.912(5)	1.915(3)
d(Cu−O)/Å[c]	1.922(3)	1.927(2)	1.940(2)	1.939(3)	1.98 (2)[a] 1.87(2)[b]	1.925(5)	1.932(2)
α(N−Cu−N)/°[d]	83.8(2)	84.1(2)	83.6(1)	97.0(2)	95.2(3)	95.6	99.9(1)
δ(C−N−Cu−N)/°[e]	0.3(2)	0.3(2)	0.6(1)	0.2(2)	7.2(1)	12.3	27.1(3)
crystal system	monoclinic	monoclinic	monoclinic	monoclinic	monoclinic	monoclinic	tetragonal
space group	*C*2/*c*	*C*2/*c*	*C*2/*c*	*C*2/*c*	*C*2/*c*	*C*2/*c*	$P4_12_12$
Cu chelate rings[f]	5−5−5	5−5−5	5−5−5	5−6−5	5−6−5	5−6−5	5−7−5
literature	16	8	18	16	9	16	this work

[a] aryl-*N*(oxamato) entity. [b] alkyl-*N*(oxamato) entity. [c] Bond length. [d] Bond angle. [e] Dihedral angle with respect to the amido carbon. [f] The ligand forms three chelate rings around the Cu(II) ion involving a certain number of atoms.

a 40% solution in MeOH, 2 mmol). After 20 min of stirring a solution of $[CuCl_2(H_2O)_2]$ (85 mg, 0.5 mmol) in MeOH (10 mL) was added dropwise. The resulting mixture was stirred for 120 min, and afterward the solvent was completely evaporated. The residue was solved in H_2O (100 mL) and extracted in CH_2Cl_2 (3 × 50 mL). The organic phase was dried with Na_2SO_4, and then the solvent was evaporated. The obtained green solid was then dried in air. Suitable crystals of **7** for X-ray crystallography were obtained from CH_2Cl_2 solutions by slow condensation of Et_2O.

Yield: 235 mg (48%) of **7**, $CuC_{56}H_{84}N_4O_6 \cdot 2H_2O$ (991.0 g/mol). Elemental analysis calculated C 67.73, H 8.95, N 5.64; found C 67.77, H 9.01, N 5.37.

2.2. Physical Measurements. Elemental analysis (C, H, N) was performed on a Vario EL from Heraeus. The EPR spectra were recorded at about 9.5 GHz (X-band) at variable temperatures, at about 34 GHz (Q-band), and at about 94 GHz (W-Band) using a Bruker E600 EPR spectrometer. If not otherwise stated, a modulation amplitude of 4 Gauss was used. The spectral simulations were performed using the program packages EasySpin[23] and Xsophe from Bruker.[24] Line broadening effects were included by convoluting the calculated line spectrum with a Gaussian line shape. The line broadening which mainly originates from the unresolved hyperfine couplings was assumed to be 0.5 mT for powder measurements. The Davies ENDOR investigations were performed at a temperature of 16 K using a Bruker Elexsys E700 FT-EPR spectrometer operating at Q-band frequencies and an ENI 300 RF amplifier.

The isotropic EPR parameters were obtained from room temperature measurements of the *bis*(oxamato) type complexes in CH_2Cl_2 with a concentration of 0.5 mg/mL. The anisotropic part of the EPR parameters was extracted from measurements of the paramagnetic complexes in a frozen solution of 0.5 mg/mL of CH_2Cl_2 in case of **7** and from diamagnetic diluted powder measurements in the cases **1**−**6** to decrease the broadening of the EPR lines. Such powders were produced dissolving 0.5% of the Cu(II) complex and 99.5% of the structurally isomorphic Ni(II) complex in MeCN. The solid was obtained by following precipitation with Et_2O.

UV−vis absorption and circular dichroism (CD) spectra at room temperature were recorded in CH_2Cl_2 (2×10^{-5} mol/L and 3×10^{-3} mol/L). For the absorption spectra, the Thermo Spectronics UV/vis spectrometer of the type "Genesys 6" was used. The CD investigations were obtained on a home-built instrument based on a JASCO J-715 spectropolarimeter.

Diffraction intensity data for single crystals of **7** were collected at temperatures of 150(2) K on a Oxford Diffraction Xcalibur3 diffractometer with Mo Kα radiation ($\lambda = 0.71073$ Å). The structure of **7** was solved using direct methods with SHELXS-97 and was refined by full-matrix least-squares on F^2 with SHELX-97.[25] All non-hydrogen atoms were refined anisotropically. All hydrogen atom positions, except for *O*-bonded hydrogen atoms, were refined using a riding model. The positions of *O*-bonded hydrogen atoms cannot be found in the difference Fourier map. The absolute structure of **7** was established by anomalous dispersion effects with respect to the absolute structure parameter.[26] Crystal parameters and structure refinements are reported in Table 2.

Table 2. Crystallographic Data for **7**·2H_2O

empirical formula	$C_{56}H_{88}N_4O_8Cu$
formula mass [g/mol]	1008.84
crystal system	tetragonal
space group	$P4_12_12$
a [Å]	12.0818(4)
b [Å]	12.0818(4)
c [Å]	37.624(2)
α [°]	90.00
β [°]	90.00
γ [°]	90.00
V [Å^3]	5492.0(4)
Z	4
$D_{calcd.}$ [g/cm^3]	1.220
μ [mm^{-1}]	0.453
$\theta_{min.}/\theta_{max.}$ [°]	0.987/25.39
reflections collected	30601
reflections unique	4987
reflections observed	2193
no. of parameters	312
$R(F)$	0.0437
$Rw(F^2)$	0.0711
S (GOF) on F^2	0.900
$\Delta\rho_{max.}/\Delta\rho_{min.}$ [e/Å^3]	0.518/−0.317
Flack parameter	−0.045(17)

2.3. Quantum Chemical Studies. Quantum chemical calculations were performed with the program packages TURBOMOLE[27,28] and ORCA[29,30] using methods of the DFT by applying the B3-LYP hybrid functional[31] with def2-TZVP[32,33] basis sets for all atom types. The two $[^nBu_4N]^+$ counterions were neglected, and the charge of the dianion was compensated by the conductor-like screening model (COSMO)[34] as in previous reports.[35,17] This leads

(21) Ruiz, R.; Barland, C. S.; Aukauloo, A.; Mallart, E. A.; Journaux, Y.; Cano, J.; Munoz, M. C. *J. Chem. Soc., Dalton Trans.* **1997**, 745.
(22) Rüffer, T.; Bräuer, B. *Anal. Sci.* **2007**, 23.
(23) Stoll, S.; Schweiger, A. *J. Magn. Reson.* **2006**, *178*, 42.
(24) Wang, D.; Hanson, G. R. *J. Magn. Reson.* **1995**, *A117*, 1.
(25) (a) Sheldrick, G. M. *Acta Crystallogr., Sect. A* **1990**, *46*, 467. (b) Sheldrick, G. M. *SHELXL-97, Program for Crystal Structure Refinement*; University of Göttingen: Göttingen, Germany, 1997.
(26) Flack, H. D. *Acta Crystallogr.* **1983**, *A39*, 876.
(27) Ahlrichs, R.; Bär, M.; Häser, M.; Horn, H.; Kölmel, C. *Chem. Phys. Lett.* **1989**, *162*, 165.
(28) *TURBOMOLE* V5-10; TURBOMOLE GmbH Karlsruhe, 2008, http://www.turbomole.com/release-notes.html.
(29) Neese, F. *J. Chem. Phys.* **2003**, *119*, 9428.
(30) Neese, F. *Int. J. Quantum Chem.* **2001**, *83*, 104.
(31) Lee, C.; Yang, W.; Parr, R. G. *Phys. Rev. B 37* **1988**, 785.
(32) Weigend, F.; Ahlrichs, R. *Phys. Chem. Chem. Phys.* **2005**, *7*, 3297.
(33) Schaefer, A.; Horn, H.; Ahlrichs, R. *J. Chem. Phys.* **1992**, *97*, 2571.

to negative energies for all occupied orbitals. All calculations were done with default settings for convergence criteria and with default parameters for the COSMO model. The EPR parameters were obtained using the flexible CP(PPP) basis set of ORCA[36] for Cu to get a good estimation for the g tensor components[37] and def2-TZVP[32,33] for all the other atoms.

The analysis of the spin population, $\rho_s(\mathbf{r})$, that is, the difference of populations of alpha and beta electrons, was done for the optimized geometry using the Mulliken population analysis,[38] the Loewdin analysis, and the Natural population analysis (NPA)[39] to obtain the number of unpaired electrons per atom, n_A (A = Cu, N, O). As an additional check, $\rho_s(\mathbf{r})$ was also integrated numerically within spheres of radius R centered at these atoms. This leads to $n_s(R)$, the number of unpaired electrons contained in a sphere of radius R around the respective atom. The radius, for which $n_s(R)$ may be identified with n_A is defined by $n_s(R)$ being stationary with respect to variation of R (see Figure 11, right panel). For an isotropic spin population this would correspond to $\rho_s(R) = 0$. For the present case showing an anisotropic distribution, this is only an approximation. Nevertheless, from the shape of the spin population (see Figure 11 below), this definition appears to be reasonable also here.

For the calculation of the magnetic coupling parameters, the broken-symmetry (BS) approach was used; for more details see ref 10 and the references therein. The calculations were performed for the corresponding trinuclear complex of **7** which was constructed by adding two $[Cu(pmdta)]^{2-}$ fragments in the terminal positions of the $[Cu(R\text{-}bnbo)]^{2-}$ entity. The bond distances and angles of the $[Cu(pmdta)]^{2-}$ fragments, and thus the τ-parameter, were exactly the same as previously used for $[Cu_3(nabo)(pmdta)_2](BF_4)_2$ (**16**)[10] to compare the effect of the central *N,N′*-bridge on the calculated J. For this purpose, the program package TURBOMOLE with the above-mentioned method was used. We have used the artificial trinuclear complex of **7** for the calculation of J since we failed up to now to grow suitable single crystals large enough for structural and magnetic measurements.

3. Results and Discussion

3.1. Structure of $[^nBu_4N]_2[Cu(R\text{-}bnbo)]\cdot 2H_2O$ (7). The crystal structure of **7** consists of discrete $(^nBu_4N)^+$ cations and $[Cu(R\text{-}bnbo)]^{2-}$ anions (**7a**), to which two water molecules are connected via hydrogen bonds. Complex **7** crystallizes in the tetragonal chiral space group $P4_12_12$. The $[Cu(R\text{-}bnbo)]^{2-}$ anion (**7a**) possesses a crystallographically induced C_2 symmetry with the C_2 axis along the Cu1 ion and the center of the C10−C10A bond. The molecular structure of **7a** is shown in Figure 2. Selected bond lengths and angles are listed in Table 3.

The Cu(II) ion of **7a** is coordinated by two deprotonated amido nitrogens and two carboxylate oxygens resulting in a $\eta^4(\kappa^2N, \kappa^2O)$ coordination. This coordination type is usually observed for related complexes of *bis*(oxamato) ligands, although exceptions have been observed.[40,41]

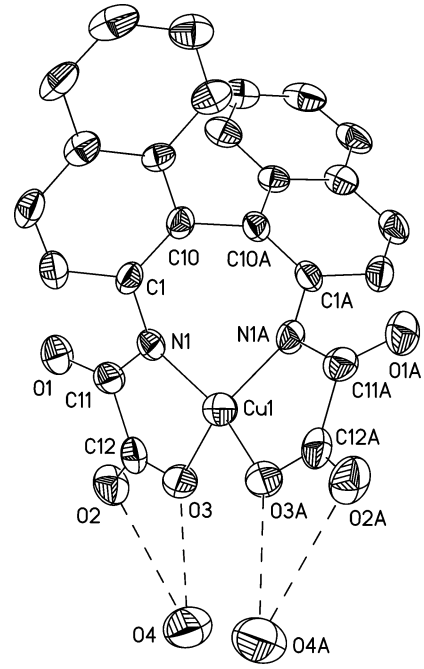

Figure 2. ORTEP-plot (50% probability level) of the molecular structure of **7a**·$2H_2O$. The H atoms have been omitted for clarity.

Table 3. Selected Bond Lengths and Angles

bond lengths/Å		bond angles/°	
Cu1−N1	1.915(3)	N1−Cu1−N1A	99.9(1)
Cu1−O3	1.932(2)	N1−Cu1−O3	85.2(1)
N1−C1	1.409(5)	N1−Cu1−O3A	158.8(1)
N1−C11	1.338(5)	O3−Cu1−O3A	97.6(1)
C11−C12	1.563(6)	C12−O3−Cu1	113.7(3)
O1−C11	1.248(5)	C1−C10−C10A	122.4(3)
O2−C12	1.220(5)	C11−N1−C1	121.3(3)
O3−C12	1.291(5)	C11−N1−Cu1	113.9(2)
O2···O4[a]	3.291(4)	C1−N1−Cu1	120.2(2)
O3···O4[a]	2.773(4)	O1−C11−N1	128.9(4)
		O1−C11−C12	119.4(4)
		N1−C11−C12	111.7(4)
		C10−C1−N1	121.0(3)
		O2−C12−C11	120.0(4)
		C11−C12−O3	114.2(4)
		O2−C12−O3	125.8(4)

[a] O4A is reported by the symmetry operation $y, x, -z$.

The CuN_2O_2 setup of structurally characterized *bis*(oxamato) type complexes with an $\eta^4(\kappa^2N, \kappa^2O)$ coordination of the central metal ion has been detected so far as almost planar, see, for example, ref 16. The highest deviation from planarity of the CuN_2O_2 setup has been observed for **6**.[16] The deviation from the N_2O_2 mean plane to which the metal atom belongs is ±0.177 Å for the N and ±0.180 Å for the O atoms resulting in a slight tetrahedral distortion of the Cu(II) environment.[16] This is furthermore confirmed by the calculation of interplanar angles of the mean planes of the oxamato groups [C11, C12, O1−O3, N1 (group I); C11A, C12A, O1A−O3A, N1A (group II)] with I:II = 13.5° for **6**.

For **7a** the related interplanar angle was calculated to be 43.8(3)° (rms deviation, 0.091 Å; highest deviation from mean plane, ± 0.144 Å for O3). Thus, the tetrahedral distortion of **7a** is larger compared to **6**[16] because of steric hindrance of the 2,2′-substituted-[1,1′-binaphthyl] ligand.

Usually, for 2,2′-substituted-[1,1′-binaphthyl] compounds, a nearly cross-arrangement of the two substituted

(34) Klamt, A.; Schüürmann, G. *J. Chem. Soc., Perkin Trans. 2* **1993**, 799.
(35) Zimmermann, C.; Anson, C. E.; Weigend, F.; Clérac, R.; Dehnen, S. *Inorg. Chem.* **2005**, *44*, 5686.
(36) Neese, F. *J. Chem. Phys.* **2001**, *115*, 11080.
(37) Atanasov, M.; Comba, P.; Martin, B.; Müller, V.; Rajaraman, G.; Rohwer, H.; Wunderlich, S. *J. Comput. Chem.* **2006**, *27* (12), 1264.
(38) Mulliken, R. S. *J. Chem. Phys.* **1955**, *23*, 1833.
(39) Reed, A. E.; Weinstock, R. B.; Weinhold, F. *J. Chem. Phys.* **1985**, *83*, 735.
(40) Rüffer, T.; Bräuer, B.; Walfort, B. *Inorg. Chem. Commun.* **2006**, *9*, 1111.

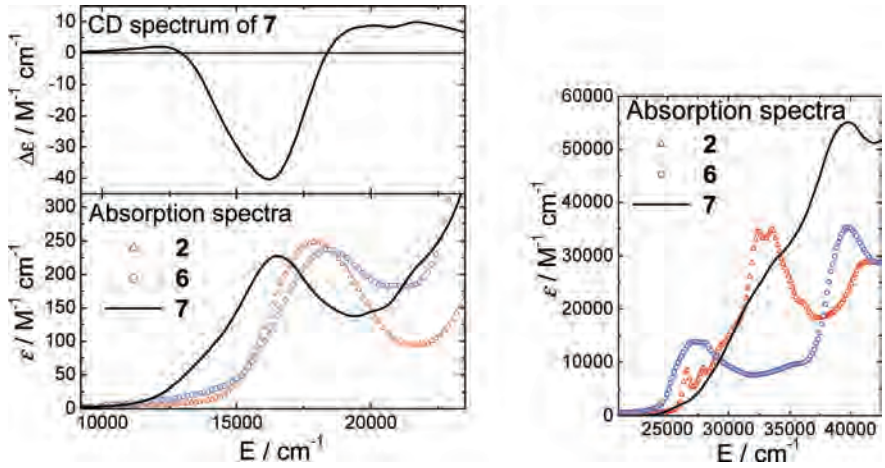

Figure 3. CD spectrum of **7** and absorption spectra of **2**, **6**, and **7**.

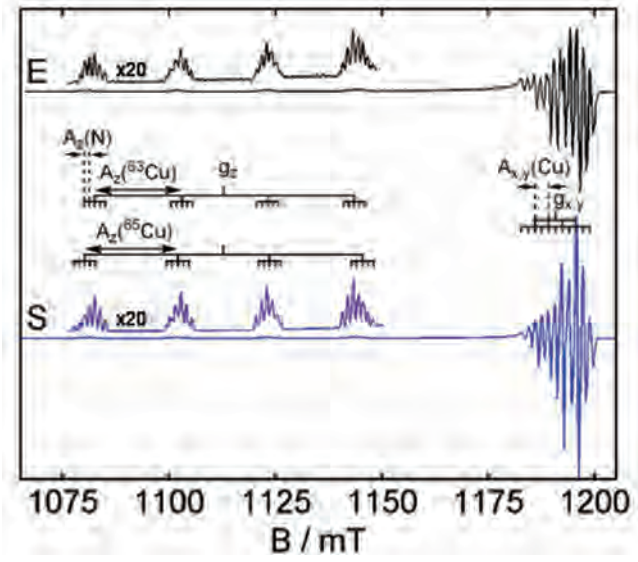

Figure 4. Experimental (E) and simulated (S) EPR spectrum of **6** at $f =$ 34.031 GHz (Q-band) and $T = 298$ K. For B_0 orientations along the z axis of the g tensor, the EPR spectra are zoomed in. The assignment of the EPR bands is given schematically.

binaphthyl groups is observed in the solid state. For the two ethyl[*N*-1-naphthyl]-2-oxamate groups of **7** and **14**, such a cross-arrangement is observed as well. The interplanar angle from calculations of the mean planes of the non-hydrogen atoms of these groups is 81.52(4)° and 83.84(2)° for the two crystallographically independent molecules of **14**.[9] The complexation of Cu decreases this angle to 74.1(3)° for **7**.

UV−vis Absorption and Circular Dichroism Studies. In the following, the absorption properties of systems which include one or more naphthyl units as a *N,N′*-bridge will be discussed. The absorption properties of **6** were taken from the literature[16] for reasons of comparison. The absorption spectra of **2**, **6**, and **7** are shown together in Figure 3. They are characterized by low-energy transitions arising from d-d transitions of Cu(II) with a d^9 electronic configuration with $d_{x^2-y^2}$ as the highest occupied molecular orbital. For **2** and **6** a square planar environment (i.e., $^2B_{1g}-{}^2A_{1g}$, $^2B_{1g}-{}^2B_{2g}$, and $^2B_{1g} - {}^2E_{1g}$ in ideal D_{4h} symmetry) can be assumed. The most intensive absorption can be found at 17900 cm^{-1} ($\varepsilon \approx 250$ M^{-1} cm^{-1}), 18400 cm^{-1} ($\varepsilon \approx 250$ M^{-1} cm^{-1}), and 16500 cm^{-1} ($\varepsilon \approx 230$ M^{-1} cm^{-1}) for **2**, **6**, and **7**, respectively. The significant red shift of the absorption maximum for **7** in comparison to **2** and **6** is due to strong deviations from the square planar coordination geometry in the case of **7**. Because **7** has a chirality axis, its CD spectrum allows distinguishing between the different d-d transitions. However, it was not possible to determine unequivocally the assignment of the transitions because the energy order of the respective orbitals is unknown. The same is valid for the transitions at higher energies arising mainly from the σ-σ^* and π-π^* transitions which vary strongly in intensity and energy position because of the different *N,N′*-bridges.

3.2. EPR Spectroscopic Investigations and Comparison with DFT Calculations. The systems **1** to **6** were investigated by EPR on powder samples diamagnetically diluted by the corresponding Ni(II) complexes **8** to **13**, respectively. Complex **7** was investigated in frozen solution because the Ni analogue cannot be prepared. To obtain the isotropic values for A and g for **1**−**7**, they were also investigated in solution using CH_2Cl_2 as solvent.

The EPR spectra were analyzed using the following spin-Hamiltonian

$$H_{sp} = \mu_B \mathbf{B}_0 \cdot \mathbf{g} \cdot \mathbf{S} + \mathbf{S} \cdot \mathbf{A}^{Cu} \cdot \mathbf{I}^{Cu} + \sum_{i=1}^{2} \mathbf{S} \cdot \mathbf{A}^{N_i} \cdot \mathbf{I}^{N_i} + H_{nuclei} \quad (1)$$

The first term is the electron Zeeman interaction with the Bohr magneton μ_B, the external magnetic field $\mathbf{B}_0$, and the g tensor $\mathbf{g}$. The second term is the hyperfine interaction between the electron spin $\mathbf{S}$ and the nuclear spin $\mathbf{I}$ of the copper nucleus (^{63}Cu, ^{65}Cu). The third term describes the hyperfine interaction of the electron spin with the two nitrogens. The last term describes the nuclear Zeeman, hyperfine, and nuclear quadrupole interactions of the surrounding nuclei. The cw-EPR spectra are dominated by the first three terms. The hyperfine and nuclear quadrupole tensors of the nitrogens and the proton couplings in H_{nuclei} can be determined using Davies ENDOR.

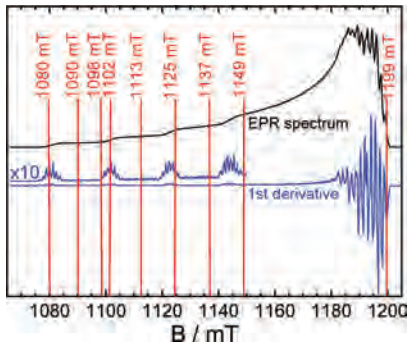

Figure 5. Experimental FID detected EPR spectrum (π/2-pulse of 200 ns) of **6** and its first derivative at $f = 34.031$ GHz (Q-band) and $T = 16$ K. The vertical lines represent the different observer positions for the respective pulse ENDOR measurements.

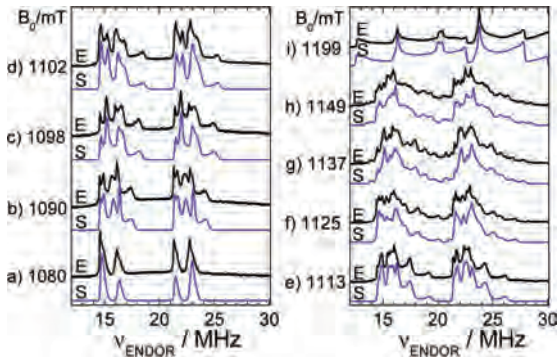

Figure 6. Experimental (E) and simulated (S) nitrogen Davies-ENDOR spectra of **6** at $f = 34.031$ GHz (Q-band) and $T = 16$ K using an RF pulse length of 35 μs. The microwave pulse lengths were 200 ns for the (soft, selective) inversion pulse and 40−80 ns for the two pulse detection sequence which had a waiting time (τ) of 300 ns. The respective observer positions are shown in Figure 5.

For the investigated complexes, the **g** and $\mathbf{A}^{Cu}$ matrices are assumed to be coaxial and axially symmetric with

$$|A_x^{Cu}| \approx |A_y^{Cu}| \approx |A_\perp^{Cu}| < |A_z^{Cu}| = |A_\parallel^{Cu}| \quad (2)$$

Figure 4 shows the measured and simulated Q-band EPR spectra on the example of complex **6**. For all the other compounds, the EPR spectra look rather similar and are not shown here. The features labeled with x, y, and z consist of a quartet ($I(^{63,65}\mathrm{Cu}) = 3/2$) of quintets ($I(^{14}\mathrm{N}) = 1$) for B_0 field orientations for which both N donor atoms are magnetically equivalent. The individual ^{63}Cu and ^{65}Cu signals are different in intensity because of their different natural abundances (^{63}Cu (69%), ^{65}Cu (31%), $g_N(^{63}\mathrm{Cu}) = 1.4804$, $g_N(^{65}\mathrm{Cu}) = 1.5860$). For B_0 orientations in the molecular xy-plane of the Cu g-ellipsoid, the spectra become more complicated because the ^{14}N quintets overlap each other as a result of the small ^{63,65}Cu hyperfine coupling.

For **6**, the orientation of the tensor principal axis system of Cu and N was investigated in detail by performing Davies ENDOR studies in the Q-band. Furthermore, this method was used to determine the hyperfine and nuclear quadrupole principal values of the nitrogens. The Davies ENDOR spectra were collected at different observer positions which are highlighted in Figure 5 as vertical lines.

The respective Davies ENDOR spectra are shown in Figure 6 and the obtained EPR parameters, that is, the principal values of

Table 4. g, A, and Q Principal Values and the Respective Euler Angles for **6**[a]

	g	A^{Cu}/MHz	A^N/MHz	Q^N/MHz	Q^N/MHz(calc.)[b]	Euler angle/°
x	2.041	95	36.3	1.28	1.21	$\alpha = 35$
y	2.041	95	50.5	−0.70	−0.70	$\beta = 14$
z	2.186	632	37.5	−0.58	−0.51	$\gamma = 0$

[a] Experimental error bars: $g(\pm 0.002)$, $A^{Cu}(\pm 3$ MHz), $A^N(\pm 0.4$ MHz), $Q(\pm 0.03$ MHz), Euler angles ($\pm 2°$). [b] B3-LYP, COSMO model, basis: CP(PPP) for Cu, def2-TZVP for all the other atoms using the Orca program.

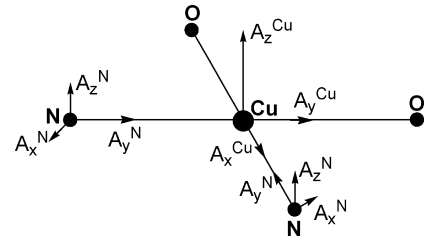

Figure 7. Schematic representation of the principal axis system for all investigated compounds.

g, $\mathbf{A}^{Cu}$, $\mathbf{A}^N$, $\mathbf{Q}^N$, and the Euler angles, are reported in Table 4. The Euler angles describe the orientations of the nitrogen hyperfine and nuclear quadrupole tensors in the **g** tensor frame. The resulting geometry of the principal axis system is illustrated in Figure 7. It was assumed that the $\mathbf{A}^N$ and **Q** tensors are collinear to each other, but they are not collinear with the **g** and $\mathbf{A}^{Cu}$ tensors. The Euler angle between the z-axes of $\mathbf{A}^{Cu}$ and $\mathbf{A}^N$ amounts to 14°. The angle between the x axes of the two reference frames amounts to 35°. Although, the angle β is quite small, it is a very sensitive parameter in the parallel region of the EPR spectrum. The difference in the EPR parameters of the two coordinating nitrogens is almost negligible. The EPR parameters are qualitatively reproduced by means of DFT calculations (see Tables 4 and 5).

To increase the spectral resolution and thus simplify the spectral analysis, W-band cw-EPR measurements were performed on all Cu complexes. Within negligible deviations in all cases, the same orientation of the A tensor, see Figure 7, was found. Moreover, for all the investigated complexes, the following assumption was taken

$$|A_x^N| \approx |A_z^N| \approx |A_\perp^N| < |A_y^N| = |A_\parallel^N| \quad (3)$$

and the two coordinating nitrogens were considered equivalent. Good agreement between the X-band EPR spectra and the simulations is obtained, as shown for **3** (see Figure 8), albeit the mentioned assumptions are rather rough as shown also from DFT calculations (Table 5), which instead predict the rhombicity of A^N.

In Figure 8, the quintets arising from the coupling of the unpaired electron with the nuclear spin of two nitrogens are clearly resolved in the parallel region of the spectrum. The peaks marked with an "x" in the left-hand side diagram result from the coupling between nitrogen and the ^{65}Cu isotope.

On the other hand, the larger resolution of the W-band EPR spectra compared to those recorded in X-band points out the limits of the assumptions taken. The simulated (S) and the experimental (E) W-band spectrum of **3** are shown in Figure 9. The signals corresponding to g_z are clearly separated from the signals corresponding to $g_\perp$. The values of g_x and g_y are assumed to be equal.

Table 5. g and A Values for **1**−**7**

	experimentally obtained values[f]					calculated values using DFT[e]			
compound	g_x	g_y	g_z	g_{iso}	g_{av}	g_x	g_y	g_z	g_{iso}
1	2.042[b]	2.042[b]	2.184[b]	2.092	2.089	2.033	2.035	2.116	2.061
2	2.041	2.041	2.180	2.092	2.087	2.034	2.037	2.115	2.062
3	2.042	2.042	2.186	2.093	2.090	2.038	2.039	2.131	2.069
4	2.045	2.045	2.185	2.096[a]	2.092	2.034	2.036	2.119	2.063
5	2.042	2.042	2.193	2.096	2.092	2.038	2.040	2.133	2.070
6	2.040	2.040	2.185	2.092	2.088	2.031	2.032	2.105	2.056
7	2.048	2.048	2.223	2.108	2.106	2.043	2.043	2.151	2.079

	experimentally obtained values[f]					calculated values using DFT[e]			
compound	$A_x(^{63}Cu)$	$A_y(^{63}Cu)$	$A_z(^{63}Cu)$	$A_{iso}(^{63}Cu)$	$A_{av}(^{63}Cu)$	$A_x(^{63}Cu)$	$A_y(^{63}Cu)$	$A_z(^{63}Cu)$	$A_{iso}(^{63}Cu)$
1	−104	−104	−617	−275	−275	−35	−40	−634	−237
2	−104	−104	−617	−275	−275	−21	−27	−637	−228
3	−99	−99	−618	−267	−270	−31	−34	−616	−227
4	−100	−100	−614	−270[a]	−271	−25	−34	−634	−231
5	−92	−92	−596	−257	−259	−11	−26	−600	−212
6	−95	−95	−632	−269	−269	−20	−25	−651	−232
7	−55	−55	−555	−220	−220	−5	−13	−564	−194

	experimentally obtained values[f]					calculated values using DFT[e]			
compound	$A_x(^{14}N)$	$A_y(^{14}N)$	$A_z(^{14}N)$	$A_{iso}(^{14}N)$	$A_{av}(^{14}N)$	$A_x(^{14}N)$	$A_y(^{14}N)$	$A_z(^{14}N)$	$A_{iso}(^{14}N)$
1	40	59.5	40	46.2	46.5	43	62	42	49
2	40	59.5	40	46.5	46.5	49	67	50	55
3	40	59.5	40	46.0	46.5	44	61	42	49
4	40	59	40	45.6[a]	45.3	45	60	44	50
5	39	51	39	43.0	43.0	39[c]	55[c]	37[c]	43[c]
						40[d]	56[d]	39[d]	45[d]
6	38	54	38	42.7	43.3	43	59	45	49
7	33	44	33	37.6	36.7	34	48	32	38

[a] In agreement with literature ref 43. [b] In agreement with literature ref 44. [c] Aromatic amine. [d] Aliphatic amine. [e] B3-LYP, COSMO model, basis: CP(PPP) for Cu, def2-TZVP for all the other atoms using the Orca program. [f] Experimental error bars: g(±0.003), $A^{Cu}(\pm 3)$, $A^{N}(\pm 2)$. A in MHz.

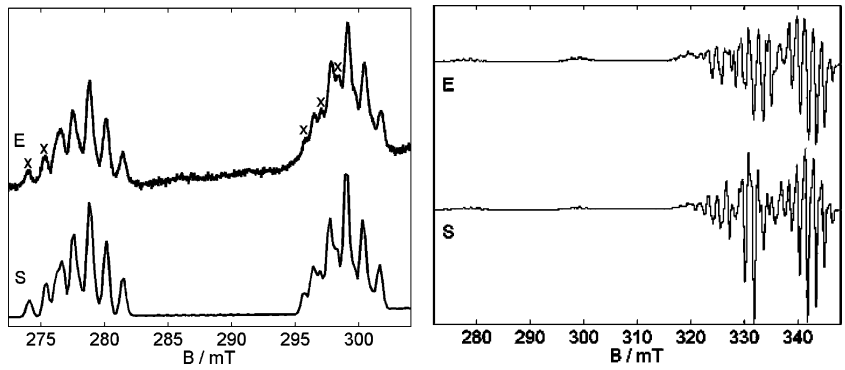

Figure 8. Experimental (E) and simulated (S) EPR powder spectrum of **3** at $f = 9.437$ GHz (X-Band) and $T = 298$ K. On the left side, the low field range is zoomed in, and the clearly seen isotope peaks are highlighted with an "x".

Simulations have shown that these parameters differ less than 0.05% from each other.

The differences between the experimental and simulated spectrum in the right panel of Figure 9 could not be minimized with the assumptions taken: the equivalence of the two nitrogens and the axial symmetry of the Cu and N hyperfine tensors.

The tensor principal values of the investigated complexes are reported in Table 5. The average values were calculated according to

$$A_{av} = \frac{1}{3}(A_x + A_y + A_z) \quad (4)$$

and

$$g_{av} = \frac{1}{3}(g_x + g_y + g_z) \quad (5)$$

They correspond very well to the values determined from the solution spectra, see isotropic values (iso) in Table 5.

The X-band EPR spectrum on solution of **6** in CH_2Cl_2 recorded at room temperature is shown in Figure 10. It shows a well-resolved four line pattern as expected for the coupling of an electron spin with the nucleus of Cu. At lower m_I values, the peak-to-peak line width Γ becomes larger. In 1966 Wilson and Kivelson[42] extensively studied EPR linewidths in liquids considering the Brownian tumbling in solution. According to this theory the line broadening, described by the peak-to-peak line width Γ, is a function of the magnetic nuclear spin quantum number m_I and can be approximated by the expression $\Gamma = A + Bm_I + Cm_I^2 + Dm_I^3$ where the parameters A, B, C, and D depend on the temperature.

(41) Zhu, Z. C.; Mao, X. P.; Xu, Z.; Huang, X. Y. *Chin. J. Struct. Chem.* **2000**, *19*, 322.
(42) Wilson, R.; Kivelson, D. *J. Chem. Phys.* **1966**, *44*, 1.

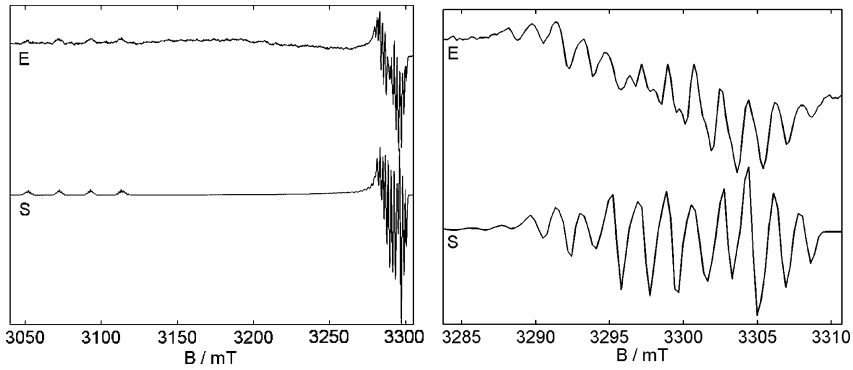

Figure 9. Experimental (E) and simulated (S) EPR powder spectrum of **3** at $f = 93.897$ GHz (W-Band) and $T = 10$ K.

The spectrum in Figure 10 was simulated using line width parameters $A = 1.625$ mT and $B = 0.65$ mT.

The EPR parameters are listed in Table 5. The signs of the hyperfine eigenvalues, which could not be obtained experimentally, were taken as properly predicted by DFT calculations. As expected, the parameters determined for the compound **7** differ significantly from those of the other compounds. This clearly demonstrates that the structural parameters, shown in Table 1, have a huge influence on the EPR parameters. The g_x, g_y, and g_z values are smaller in the more or less square planar compounds **1**−**4** compared to the tetrahedrally distorted complex **7**. In contrast, the respective hyperfine values A for Cu(II) and N are larger for the square planar complexes compared to the tetrahedrally distorted one.

The qualitative trends in g arise from a decrease in the energy separation of the electronic levels when going from square planar to tetrahedral by distorted structures. The same effect is expected to cause the decrease of the absolute value of A^{Cu} values.

The EPR parameters resulting from quantum chemical calculations are reported in Table 5. The experimental trends of the EPR parameters were reproduced. The calculated g values are smaller than those experimentally determined but differ from the experimental values by less than 0.01 in the case of g_x and g_y and by less than 0.07 for g_z. The absolute values of A^N are up to 20% too high, and A_z^{Cu} meets the experimental values with deviations smaller than 5%. The highest deviations arise from A_x and A_y for Cu for which the experiment leads from 4 up to 5 times higher values. Such high deviations were already reported for other Cu(II) transition metal complexes.[45] Some reasons for this behavior are given in, for example, refs 46, 47 and some new approaches are reported in refs 47, 48.

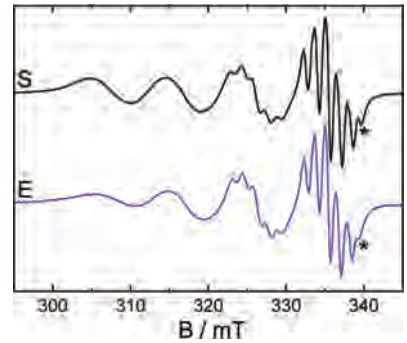

Figure 10. Experimental (E) and simulated (S) EPR spectrum of **6** in CH_2Cl_2 at $f = 9.438$ GHz (X-Band) and $T = 298$ K. The band resulting from the interaction with ^{65}Cu is highlighted with a "*".

3.3. Experimental and Theoretical Studies of Spin Population. Considering Cu(II)-*bis*(oxamato) type molecules as building blocks for molecule based magnets, the calculation of spin populations seems to be straightforward with respect to the interpretation of magnetic coupling phenomena of the corresponding multinuclear transition metal complexes. To get insights into the delocalization of the spin population on the Cu complex and into its trend over the different complexes, simplified models are used to extract the spin population from the experimentally determined hyperfine tensors.

The hyperfine tensor **A** can be written as the sum of the isotropic or Fermi contact contribution $\mathbf{A}_{iso}$, the spin dipolar contribution $\mathbf{A}_{dip}$, and the orbit dipolar contribution $\mathbf{A}_L$. $\mathbf{A}_{iso}$ is given by the sum of the unpaired spin population determined by the unpaired electron in an s orbital and the spin polarization of the inner s orbitals.[49] The $\mathbf{A}_{dip}$ term is determined by the dipolar interaction between the electron and the nuclear spin. A more detailed description of the terms can be found in literature.[50]

For complex **7**, a compressed regular tetrahedron is assumed leading to $d_{x^2-y^2}$ as the highest occupied molecular orbital of the Cu(II) ion.[51] For the complexes **1**−**6**, square planar coordination geometry is assumed. The observation that $g_z > g_x \approx g_y$ and $|A_z| > |A_x| \approx |A_y|$ for Cu(II) implies a b_{1g} ground state. According to the definition of the x and y axes given for Cu in Figure 7, the relevant molecular orbitals

(43) Wang, Q. L.; Zhao, B.; Liao, D. Z.; Yan, S. P.; Cheng, P. *Trans. Met. Chem.* **2003**, *28*, 326.
(44) Unamuno, I.; Gutiérrez-Zorrilla, J. M.; Luque, A.; Román, P.; Lezama, L.; Calvo, R.; Rojo, T. *Inorg. Chem.* **1998**, *37*, 6452.
(45) Finazzo, C.; Calle, C.; Stoll, S.; Doorslaer, S. V.; Schweiger, A. *Phys. Chem. Chem. Phys.* **2006**, *8*, 1942.
(46) Szilagyi, R. K.; Metz, M.; Solomon, E. I. *J. Phys. Chem. A* **2002**, 106–2994.
(47) Deeth, R. J. *J. Chem. Soc., Dalton Trans.* **2001**, 664.
(48) Atanasov, M.; Daul, C. A.; Rohmer, M.-M.; Venkatachalam, T. *Chem. Phys.* **2006**, 427–449.
(49) McGarvey, B. R. *J. Phys. Chem.* **1967**, *71*, 51.
(50) Bencini, A.; Gatteschi, D. *J. Am. Chem. Soc.* **1983**, *105*, 17–5535.
(51) Lohr, L. L.; Lipscomb, W. M. *Inorg. Chem.* **1963**, *2*, 911.

using the simplified assumption of D_{4h} symmetry[52] are

$$b_{1g} = \alpha d_{x^2-y^2} - \frac{\alpha'}{2}(-\sigma_1^x + \sigma_2^y + \sigma_3^x - \sigma_4^y) \quad (6)$$

for which the subscripts 1−4 denote the hybrid σ orbitals of the coordinated heteroatoms. The copper hyperfine values can be expressed as

$$\begin{aligned} A_{\parallel} &= P\left(-\kappa - \frac{4}{7}\alpha^2 + \Delta g_{\parallel} + \frac{3}{7}\Delta g_{\perp}\right) \\ A_{\perp} &= P\left(-\kappa + \frac{2}{7}\alpha^2 + \frac{11}{14}\Delta g_{\perp}\right) \end{aligned} \quad (7)$$

where $P\kappa$ is the Fermi contact term, $P(^{63}\mathrm{Cu}) = \mu_B g_e \mu_n g_n \times \langle r^{-3} \rangle = 1164$ MHz is the dipolar hyperfine coupling parameter of the unpaired electron, and $\Delta g_{||,\perp} = g_{||,\perp} - 2.0023$. From eq 7 and the experimental Cu hyperfine couplings, the values of κ and α^2 can be obtained. The parameter α^2 is the covalency parameter which describes the in-plane metal−ligand σ bonding and results in $\alpha^2 = 1$ for a pure ionic bonding and $\alpha^2 < 1$ when a covalent part contributes to the bonding. The normalization of the b_{1g} orbital yields

$$\alpha^2 + \alpha'^2 - 2\alpha\alpha' S = 1 \quad (8)$$

with the overlap integral

$$S = \frac{1}{2}\langle d_{x^2-y^2} | (-\sigma_1^x + \sigma_2^y + \sigma_3^x - \sigma_4^y) \rangle \quad (9)$$

In the literature the overlap integrals were calculated for a ligand-to-metal distance of 1.92 Å leading to overlap integrals $S(\mathrm{N}) = 0.093$ and $S(\mathrm{O}) = 0.076$ for nitrogen and oxygen, respectively.[52] The distance differs slightly for different compounds but the influence on the calculated overlap integrals is negligible. Equation 8 was used to determine the $(\alpha'/2)^2$ values from the α^2 values. Both are given in Table 6.

From the Fermi contact term, the spin population in the s orbital of each nitrogen was determined using the relation

$$\rho^{\mathrm{N}} = A_{\mathrm{iso}} / a_0 \quad (10)$$

with $a_0 = 1538.22$ MHz, which is the calculated isotropic hyperfine value for unitary electron spin population in the nitrogen s orbital.[53] The ρ^{N} values are given in Table 6 and do correlate well with the $(\alpha'/2)^2$ using the relation[45]

$$\rho^{\mathrm{N}} \approx \frac{1}{3}(\alpha'/2)^2 \quad (11)$$

Furthermore, the values obtained for the spin population on the Cu ion are compared with those deduced by the procedure of Morton and Preston.[53] The so calculated spin populations are reported in Table 6. These authors used the approach that the spin populations in the s and p orbitals (d orbitals for copper) are proportional to the isotropic (A_{iso}) and the dipolar ($A_{\mathrm{dip}} = A_{\mathrm{iso}} - A_{\perp}$) hyperfine coupling constants, respectively. In the literature[53] the proportional constants were calculated for many abundant nuclei from Hartree−Fock−Slater atomic orbitals using the Hermann−Skillman wave function.

Table 6. Spin Population (in %) for Cu (α^2) and N ($(\alpha'/2)^2$) for the Compounds under Investigation

compound	atom	α^{2a}	α^{2b}	atom	$(\alpha'/2)^{2a}$	ρ^{N}(s orbital)[a]	$(\alpha'/2)^{2b}$
1	Cu	71.0	54.6	N	10.3	3.0	14.5
2	Cu	70.5	54.6	N	10.4	3.0	14.3
3	Cu	71.8	55.8	N	10.1	3.0	14.7
4	Cu	71.1	54.8	N	10.3	3.0	14.6
5	Cu	73.0	53.8	N	10.1	2.8	9.6
6	Cu	72.9	57.6	N	9.6	3.2	12.3
7	Cu	74.0	52.6	N	9.2	2.4	7.8

[a] According to eqs 7, 8, and 10. [b] According to ref 53.

Table 7. Spin Population (Given in %) for **2**, **5**, and **7** Obtained from DFT Studies

	Mulliken			Loewdin			NPA			integrated spin population		
	Cu	N	O	Cu	N	O	Cu	N	O	Cu	N	O
2	55	15	7	62	10	6	74	8	4	64	12	6
5[a]	57	12	7	63	8	6	75	7	4	65	10	6
5[b]		14	8		10	7		7	5		11	7
7	57	11	8	63	8	6	73	6	5	64	9	7

[a] aryl-*N*(oxamato) entity. [b] alkyl-*N*(oxamato) entity.

For the complexes **1**−**4**, with a more or less square planar coordinated Cu(II) ion, a spin population on Cu(II) from 70.5 to 71.8% was found. For **5**−**7**, the spin population on the Cu(II) ion ranged from 72.9 to 74.0%; the increase is due to the deviation from square planar coordination geometry and had its maximum for the distorted tetrahedrally coordinated Cu(II) ion in **7**. The values of the spin populations agree well with the values measured by polarized neutron diffraction of similar Cu(II)-*bis*(oxamato) complexes, [15] as well as with Cu(II)-phthalocyanines investigated by means of EPR.[45] The opposite trend was calculated for the spin population on the coordinated heteroatoms which is obvious since the normalization condition given in equation 8 was used. The obtained spin population for the tetrahedrally distorted complex **7** (9.2%) is smaller compared to that of the more or less square planar complexes **1** to **4** (10.1 to 10.4%), see Table 6. Similar results were obtained for Cu(II)-phthalocyanines.[45]

The model of Morton and Preston[53] seems to overestimate the spin delocalization from Cu(II) to the coordinated heteroatoms, that is, the degree of covalency of the bonding is too high. Following this model, the values for the spin population on Cu(II) in the range of 52.6 to 57.6% are much smaller than expected and give no clear trend. In the case of N, the expected trend can be verified, that is, a higher spin population on N when the coordination geometry is more or less square planar. Using the approach of Morton and Preston, the spin population on N can be derived from the hyperfine coupling parameters of N, that is, independently of the spin population on the Cu(II) ion, and consequently no D_{4h} symmetry has to be assumed in this case.

The spin populations of **2**, **5**, and **7** were calculated with the quantum chemical methods specified in the Experimental Section and are given in Table 7. Qualitatively all the theoretical methods used show the same trends of the spin population in agreement with those experimentally obtained. The unpaired electron is mainly localized at the Cu(II) ion. The highest relative contribution from the Cu ion was obtained with the NPA (73−75%), the lowest for the

(52) Kivelson, D.; Neiman, R. *J. Chem. Phys.* **1961**, *35*, 149.

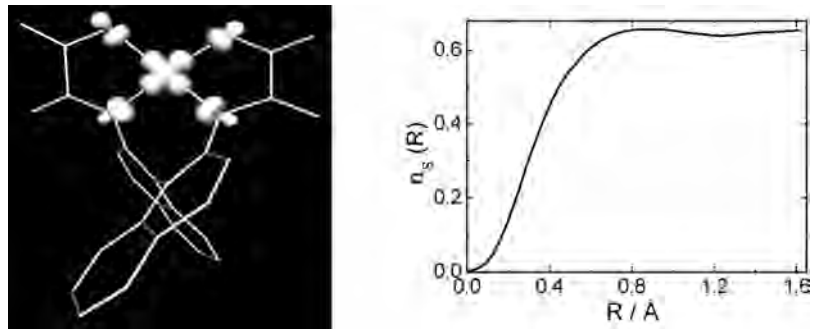

Figure 11. Spin population of **7**. Iso-surfaces are drawn at 0.01 electrons/Bohr^3 (left). Dependence of the number of unpaired electrons $n_s(R)$ on Cu within a sphere of radius R versus R (right).

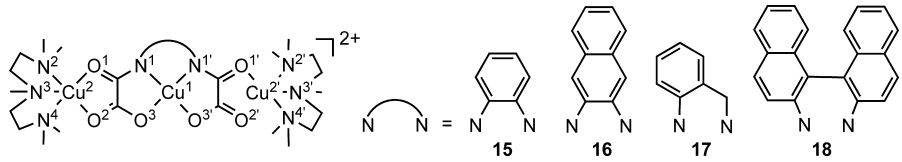

Figure 12. Chemical structures of **15** to **18** without counterion.

Table 8. Integrated Spin Population of **1** in Comparison with **15** Given in %

	1	**15**
Cu1	64	65
Cu2/2′		63
N1/1′	12	12
N2/2′, N4/4′		9
N3/3′		11
O1/1′	6	6
O2/2′		6
O3/3′		1

Mulliken analysis (55−57%), and the other methods under study yield values in between. The spin population calculated on N is higher than on O because of the stronger N−Cu bond, which correlates with the smaller Cu−N distances compared to the Cu−O distances, see Table 1.

The spin population, ρ_s, for **7** is plotted in Figure 11; iso-density surfaces are shown for $\rho_s = 0.1(0.01)$ electrons/Bohr^3. A clear localization of the spin population on the Cu, N, and O atoms is observed. The unpaired electrons occupy the d-orbital pointing to the surrounding N and O atoms and p orbitals of the latter pointing to the central Cu atom.

3.4. Correlations with Structural Parameters. In the following, some conclusions will be derived regarding the influence of the spin population distribution in the mononuclear complexes as starting materials for the corresponding trinuclear complexes, see Figure 12. DFT calculations of the spin population were performed for **1** and **15** using the same method and basis set, see Experimental Section. The numbering scheme of the Cu(II) ions will be used for all the other trinuclear complexes as well. The calculations indicate that the spin population on the central Cu(II) ion and the coordinated nitrogens remains almost unchanged when going from the mononuclear to the trinuclear complexes, see Table 8. This fact is a prerequisite for the following discussion.

Because the spin population distributions of **1** and **2** are almost identical, the same must hold also for the respective trinuclear complexes **15** and **16**. However, the experimentally determined J parameters of **15** and **16**, see Table 9, are noticeably different. The difference was supposed to originate from packing effects influencing the geometry of the terminal $[Cu(pmdta)]^{2+}$ fragments, reflected by the τ parameter.[8] Therein, the τ parameters of the 5-fold coordinated Cu(II) ions were calculated from the largest minus the second largest bond angle, and the difference was then divided by 60°. Therefore, the spin population distributions of the mononuclear complexes **1** and **2** cannot lie at the origin of the different J parameters of the trinuclear complexes **15** and **16**. This finding clearly indicates that the deviations from the ideal trigonal bipyramidal coordination geometry of the terminal $[Cu(pmdta)]^{2+}$ fragments are the main factors responsible for the difference in the J parameters, supporting the assertion proposed in the literature.[8]

To study the relation between structural parameters, the spin population on the heteroatoms, and the corresponding J parameter, we have predicted the J of $[Cu_3(R\text{-bnbo})(pmdta)_2]^{2+}$ (**18**) using the bond lengths and angles of the $[Cu(pmdta)]^{2-}$ fragments of **16**. For **18** the obtained values are $J_{12} = -141$ cm^{-1} and $J_{12'} = -150$ cm^{-1}. The average J value is given in Table 9. In ref 10 it was shown that the trends in J can be predicted with high accuracy for Cu(II)-*bis*(oxamato) complexes using the broken symmetry approach. It can thus be reliably stated that the values $J_{12} = -166$ cm^{-1} and $J_{12'} = -169$ cm^{-1} calculated for $[Cu_3(nabo)(pmdta)_2]^{2+}$ are significantly larger than that of **18**, the relative difference being well above the accuracy of the calculations. Because the coordination geometry of the terminal ligands was the same for the two considered complexes, only the distortion from the square planar coordination geometry and thus the spin population distribution can be responsible for the predicted trend. For the used method and basis set, the theoretical values are larger than the experimental values by a factor of 1.49[10] which will be used for correcting the predicted J value of **18**.

Only when the coordination geometry of the terminal ligands, and thus its τ-parameter, remains unchanged the

(53) Morton, J. R.; Preston, K. F. *J. Magn. Reson.* **1978**, *30*, 577.

Table 9. Calculated and Experimental J Values of **15**−**18**

	experiment		normalized J	DFT calculated	
	J/cm^{-1}	τ -parameter	$J(\tau = 0.4)$/cm^{-1}	J_{calc}/cm^{-1}	J_{calc}/1.49 cm^{-1}
15	−89 [8]	0.2 [8]	−113	−135 [10][a]	−91
16	−113 [8]	0.40 [8]	−113	−168 [10][a]	−113
17	−111 [9]	0.47 [9]	−104	−165[c]; −219[d] [this work]	−111[c]; −147[d]
18				−146 [this work][b]	−98

[a] Single point energy calculation of the X-ray structures. [b] Single point energy calculation of the structure of **7** assembled with the $[Cu(pmdta)]^{2+}$ entities of **16**. [c] aryl-*N*(oxamato) entity. [d] alkyl-*N*(oxamato) entity.

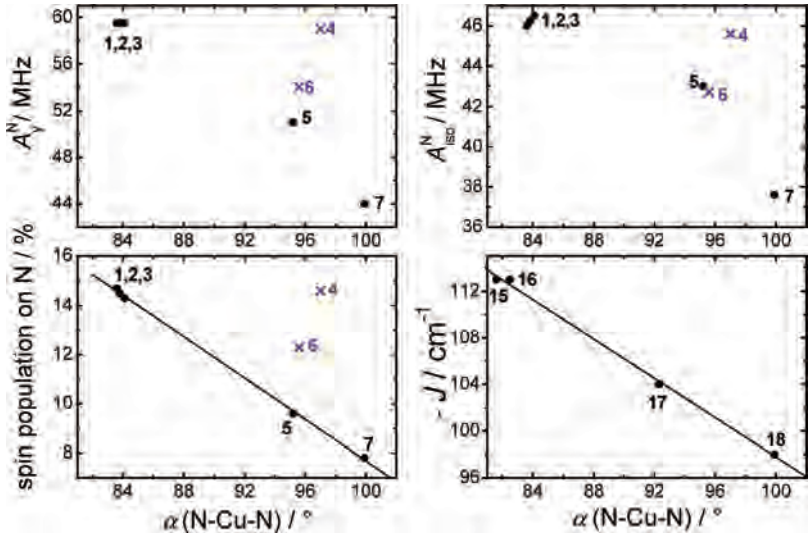

Figure 13. Dependence of the hyperfine coupling parameter of N, the spin population on N (calculated according to ref 53), and the J parameter (for τ = 0.4) on the N−Cu−N angle.

structural influences on the spin population of the N atoms coordinated to Cu(1) can be studied. For this purpose a linear dependency $\Delta J/\Delta\tau = -(120 \pm 20)$ cm^{-1} found for **15** and **16** was used to normalize the experimental J values of **15** to **17**. The extracted J values are given in Table 9 and are plotted in Figure 13.

Because **17** has an asymmetric *N,N′*-bridge with different spin densities on the nitrogen atoms bonded to the aryl and to the CH_2 group, the J_{12}, between Cu^1 and Cu^2, and the $J_{12'}$, between Cu^1 and $Cu^{2'}$, respectively, are expected to deviate from each other. From the magnetic susceptibility results it was not possible to determine the exact values of the two different J parameters. The J parameter of −111 cm^{-1}, roughly estimated from the experimental data, should be regarded as an "average" value of J_{12} and $J_{12'}$. In this work, quantum chemical calculations of J of **17** were performed leading to $J_{12}/1.49 = -111$ cm^{-1} and $J_{12'}/1.49 = -147$ cm^{-1}. J_{12} is smaller than $J_{12'}$ corresponding to the lower spin density on the nitrogen atom bonded to the aryl group. Because the nitrogen coordinated to Cu^1 is bonded to an aryl group in the case of **15**, **16**, and **18** for **17**, only the $J_{12}/1.49 = -111$ cm^{-1}, that is, the magnetic superexchange coupling mediated by the aryl bonded oxamato group, was considered in Figure 13.

The N−Cu−N bond angle was found to be the best parameter for visualizing the correlation between the spin population on N, the J parameter, and the structural variations in the complexes under study, as shown in Figure 13. This statement holds for the complexes **1**, **2**, **3**, **5**, and **7**, whereas for **4** and **6** deviations were observed. To recall, **1**, **2**, and **3** consist of fused 5−5−5 chelate rings, whereas **4**, **5**, and **6** of 5−6−5 chelate rings, and **7** of 5−7−5 chelate rings. Cervera et al. [16] reported a stronger ligand field, that is, a stronger metal−ligand-σ-bonding destabilization of the singly occupied molecular orbital (SOMO) of Cu(II), associated with the six- compared to the five-membered chelate rings leading to differences in the absorption spectra. The EPR parameters are associated with the absorption behavior by the spin−orbit coupling. The deviations from the trends shown in Figure 13 for the complexes **4** and **6** are most probably related to such effects. Influences of the atom number in coordinated chelate rings were already reported for some other systems,[54] changing the spin population distribution in such systems. The spin population in Figure 13 was derived according to ref 53 and is outlined in Table 6. The method of Morton et. al[53] was chosen because it enables one to determine the spin population on N using the hyperfine coupling parameters of N, independently of the spin population and its experimental error on the Cu center.

Because the A_y and A_{iso} of N are included in the equation for the spin population calculation on N, these plots are shown as well. Deviations from the linear dependence on the N−Cu−N bond angle for **4** and **6** can be found also for g and A^{Cu} but are not shown here.

The absolute values of the spin population on N of the precursor and the corresponding J parameter of the trinuclear complex increase when the bond angle decreases. This shows a direct correlation of these parameters.

(54) Kirmse, R., Stach, J. *ESR-Spektroskopie*; Akademie-Verlag: Berlin, 1985.

3.5. Summary and Conclusions

With compound **7**, an enantiopure Cu(II)-*bis*(oxamato) complex has been synthesized. Its excellent solubility in common organic solvents is a good prerequisite for the synthesis of molecule based magnetic compounds. Because of the extremely high tetrahedral distortion induced by the *N,N′*-bridge, **7** is a valuable system for bench-marking theoretical studies.

The excellent resolution in cw-EPR as well as in pulse-ENDOR for diamagnetically diluted powders of the investigated Cu(II) complexes allows the determination of all tensor components of **g**, **A**, and **Q** leading to a valuable insight into the magnetic properties of such complexes. The principal values of the *g* tensor are smaller for the more or less square planar compounds **1**−**4** compared to that for the tetrahedrally distorted complex **7**, while the opposite case holds for the *A* tensor principal values. This effect arises from the decrease in the energy separation of the electronic levels when going from square planar to tetrahedrally distorted structures.

Knowledge about these parameters enables the determination of the spin population distribution in the mononuclear complexes **1**−**7** and thus enables one to extract information about the main mechanisms responsible for the magnetic coupling of the respective multimetalic compounds. The comparison of the EPR and DFT results, for the complexes **1**−**7**, shows that the spin delocalization decreases when going from the square planar to the tetrahedral coordination geometry.

The results of this work suggest similar coupling parameters for multimetallic complexes in which **1** and **2** are used as building blocks. Indeed, the different antiferromagnetic couplings previously observed for the trinuclear complexes **15** and **16** based on **1** and **2**,[8] respectively, were now indirectly proved to originate from packing induced structural effects. Experimental and theoretical studies of **15** to **18** have shown a linear dependence of the *J* parameter on the N−Cu−N bond angle. The studies of their precursors **1**, **2**, **5**, and **7** suggest that an increase in the spin population on N may increases the antiferromagnetic superexchange interaction in the corresponding trinuclear complexes. However, to certainly prove this indication additional studies on a larger number of complexes are necessary.

Acknowledgment. B. Bräuer thanks the Fonds der Chemischen Industrie and the Marie Curie program for two fellowships, Prof. Wolfgang Lubitz for the opportunity to do a research visit in his group in Mülheim, and Fabrice Pointillard from Rennes for fruitful discussions. We thank Dr. Eckhard Bill and Andreas Göbels for the Circular Dichroism measurements. M. Fittipaldi acknowledges financial support by the Ministero dell'Istruzione, dell'Università e della Ricerca (MIUR), Italy.

Supporting Information Available: X-ray crystallographic file in CIF format. This material is available free of charge via the Internet at http://pubs.acs.org.

IC702460T